Nanoscale Res Lett (2009) 4:926–931
DOI 10.1007/s11671-009-9342-6

NANO EXPRESS

One-Pot Reaction and Subsequent Annealing to Synthesis Hollow Spherical Magnetite and Maghemite Nanocages

Wei Wu · Xiangheng Xiao · Shaofeng Zhang · Hang Li · Xiaodong Zhou · Changzhong Jiang

Received: 24 April 2009 / Accepted: 5 May 2009 / Published online: 22 May 2009

Abstract Water-soluble hollow spherical magnetite (Fe_3O_4) nanocages (*ca.* 100 nm) with high saturation magnetization are prepared in a one-pot reaction by sol-gel method and subsequent annealing to synthesise the maghemite (γ-Fe_2O_3) nanocages with similar nanostructures. The nanocages have been investigated by powder X-ray diffraction (XRD), transmission electron microscope (TEM), high-resolution transmission electron microscope (HRTEM), and superconducting quantum interference device (SQUID). The results indicated that glutamic acid played an important role in the formation of the cage-like nanostructures.

Keywords Magnetite · Maghemite · Sol-gel growth · Nanocages

Introduction

Magnetic nanoparticles are of great interest to researchers for their wide range a board of applications, including magnetic fluid, data storage, catalyst and biotechnology, owing to their unique magnetic properties such as superparamagnetic, low Curie temperature, and high coercivity, high susceptibility. [1]. Currently, magnetic nanoparticles are used in important biological applications, mainly including magnetic bioseparation and detection of biological entities such as cell, protein, nucleic acids, enzyme, bacterials, and virus. [2, 3]. To this end, magnetic iron oxide nanoparticles have become strong candidates, and the application of small iron oxide nanoparticles in in vitro diagnostics has been practiced for nearly half a century [4, 5]. In addition, magnetite (Fe_3O_4), maghemite (γ-Fe_2O_3) and hematite (α-Fe_2O_3) are promising and popular candidates since biocompatibility has been obtained. Usually, different biological applications require different morphologies and size of magnetic nanoparticles. Moreover, magnetic colloid particles offer attractive possibilities in bioseparation or biodetection and they should be made at dimensions comparable to those of a virus (20–500 nm), a protein (5–50 nm), or a DNA (10–100 nm) [6–10].

The internal structure and the external morphology of iron oxide nanoparticles have a significant influence on their practical applications. Particularly, the polymorphic nature of iron oxides and phase-transition studies in the nanoscale regime have attracted much attention due to its widely applications. Therefore, it is important to develop facile methods to regular both their surface morphology and size. However, it is still a technical challenge to control the size, shape, dispersibility and stability of iron oxide nanoparticles. Several preparation methods have also been reported on the synthesis of high quality of iron oxide nanoparticles, including co-precipitation, thermal decomposition, microemulsion, hydrothermal synthesis, and sono-chemical method. [11, 12]. In these methods, co-precipitation was often employed for obtaining water-soluble and biocompatible iron oxide nanoparticles, but this method presents low control of the particle shape, generates broad size

W. Wu · C. Jiang (✉)
Key Laboratory of Acoustic and Photonic Materials and Devices of Ministry of Education, Wuhan University, 430072 Wuhan, People's Republic of China
e-mail: czjiang@whu.edu.cn

W. Wu · X. Xiao · S. Zhang · H. Li · X. Zhou · C. Jiang
Department of Physics, Wuhan University, 430072 Wuhan, People's Republic of China

W. Wu · X. Xiao · C. Jiang
Center of Electron Microscopy, Wuhan University, 430072 Wuhan, People's Republic of China

distributions, and cannot avoid aggregation. Thermal decomposition and microemulsion are generally stabilized in an organic solvent by surfactants. The hydrothermal synthetic route often requires high temperature and pressure [13]. Moreover, it is important to note that using these methods at is difficult to obtain >50 nm iron oxide nanoparticles in a one-pot reaction without extra coating or seed-mediate processes [14].

Furthermore, hollow iron oxide nanoparticles have large surface area and low material density, and these nanoparticles could be potential lightweight structure materials and can be utilized for catalysis or drug-delivery. Titirichi and co-workers reported the diameter of *ca.* 500 nm hollow iron oxide microspheres by the hydrothermal approach [15], and recent progress has shown that hollow magnetite nanoparticles can be synthesized by controlling oxidation of Fe-Fe_3O_4 nanoparticles [16]. Yu et al. also reported that cage-like Fe_2O_3 hollow spheres were fabricated by the template route [17]. Herein, we report a facile and controlled synthesis of *ca.* 100 nm hollow magnetite and maghemite nanocages with uniform spherical morphology by a one-pot reaction via the sol-gel method (Fig. 1). To the best of our knowledge, there have been, so far, a few reports using finely controlled synthesis of magnetite nanocages with spherical morphology and using a one-pot sol-gel technology. Such a synthetic route is expected to have potential applications in other materials.

Experimental

Materials

Ferrous sulfate ($FeSO_4 \cdot 7H_2O$, AR) and potassium hydroxide (KOH, AR) were purchased from Tianjin Kermel Chemical Reagent CO., Ltd., potassium nitrate (KNO_3, AR) was purchased from Beijing Hongxing Chemical Reagent CO., Ltd., ethanol (C_2H_5OH, 95%, AR) and L(+)-glutamic acid ($C_5H_9NO_4$, BR) were purchased from Sinopharm Chemical Reagent CO., Ltd., and all were used as received. The MagneticSphere Technology magnetic separation stand (MSS), purchased from Promega (Z5333), was used to separate magnetic particles using washing and selecting steps.

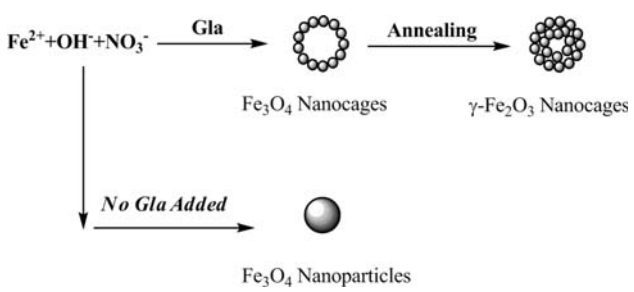

Fig. 1 Schematic figure depicting the synthesis processes of hollow iron oxide nanocages

Preparing Hollow Spherical Magnetite Nanocages

For the synthesis of hollow spherical magnetite nanocages, in a typical synthesis, solution A was prepared by dissolving 2.02 g KNO_3 and 0.28 g KOH in 50 mL double distilled water; solution B was prepared by dissolving 0.070 g $FeSO_4 \cdot 7H_2O$ in 50 mL double distilled water. Then, the two solutions were mixed together under magnetic stirring at a rate of *ca.* 400 rpm. Two minutes later, solution C [prepared by dissolving 0.18 g glutamic acid (Gla) in 25 mL double distilled water] were added dropwise into the mixed solution. The reaction temperature was raised incrementally to 90 °C and kept for 3 h under argon (Ar) atmosphere. Meanwhile, the brown solution was observed to change black. After the mixture was cooled to room temperature, the precipitate products were magnetically separated by MSS, washed with ethanol and water two times, respectively, and then redispersed in ethanol (sample 1, S1). The same preparing process without added any Gla was used to obtained the sample 3 (S3).

Preparing Hollow Spherical Maghemite Nanocages

Precipitate S1 was subjected to a series of isochronal annealing at 500 °C (sample 2, S2) for 2 h in oxygen atmosphere, and the heating rate was 5 °C/min.

Characterization

XRD patterns of the samples were recorded on a D8 Advance X-ray diffractometer using Cu Kα radiation ($\lambda = 0.1542$ nm) operated at 40 kV and 40 mA. For TEM observations, S1 and S3 (powder samples redissolved in ethanol) were dropped on copper grids and observed on a JEOL JEM-2010 (HT) transmission electron microscope at an acceleration voltage of 150 kV. For HRTEM observations, S1 and S3 (the annealed powders redissolved in ethanol) were dropped on copper grids and observed on a JEOL JEM-2010 (FEF) field-emission transmission electron microscope at an acceleration voltage of 200 kV. Magnetic measurements were performed using a Quantum Design MPMS XL-7 SQUID magnetometer. The powder sample was filled in a diamagnetic plastic capsule, and the packed sample was then put in a diamagnetic plastic straw and impacted into a minimal volume for magnetic measurements. Background magnetic measurements were checked for the packing material. Fourier transform infrared spectrum (FT-IR) measurement was carried out on a Nicolet 5700 FT-IR Spectrometer. Vacuum-dried S1 samples were mixed

and compressed with KBr to obtain pellets for FT-IR analysis.

Results and Discussion

Figure 2 shows the X-ray diffraction (XRD) patterns of Fe_3O_4 nanocages (S1, curve a) and γ-Fe_2O_3 nanocages (S2, curve b). The (220), (311), (400), (422), (511), and (440) diffraction peaks observed at curves can be indexed to the cubic spinel structure, and all peaks are in good agreement with the Fe_3O_4 phase (JCPDS card 19-0629 is also shown in the bottom of Fig. 2, blue line) and the γ-Fe_2O_3 phase (JCPDS card 39-1346 is also shown in the bottom of Fig. 2, red line), respectively. Maghemite can be prepared by the oxidation of magnetite under air at $T = 523$ K. This result reveals that the phase changes are in the direction of magnetite to maghemite, and the width of the diffraction line of S2 increases, owing to the annealing treatment [18].

The obvious electron-density differences between the dark edge and pale center of Fig. 3 further confirms the hollow interiors clearly. Figure 3a, b displays the TEM images of the Fe_3O_4 and γ-Fe_2O_3 nanocages…. It was found that the Fe_3O_4 nanocages had a hollow structure and the overall diameter of the nanocages is around 100 nm, which indicated an oriented aggregation of small Fe_3O_4 nanoparticles. One can see that the shape and size of the γ-Fe_2O_3 nanocages are similar to those Fe_3O_4 nanocages. However, the size of the central hole of nanocages becomes smaller after annealing, owing to the thermal diffusion of the small nanoparticles. The selected-area electron diffraction (SAED) pattern in the insert of Fig. 3a, b reveals the polycrystal-like feature of the samples, and their pattern agree well with the structure planes of iron oxide nanocages. When $FeSO_4$ and KOH mixed together,

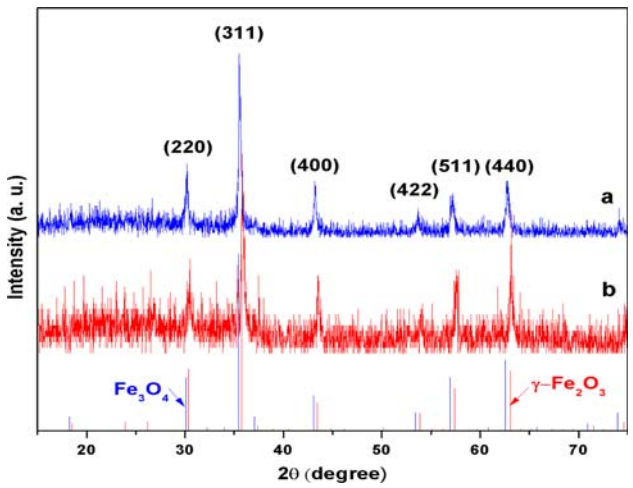

Fig. 2 XRD pattern of Fe_3O_4 nanocages (**a**) and γ-Fe_2O_3 nanocages (**b**)

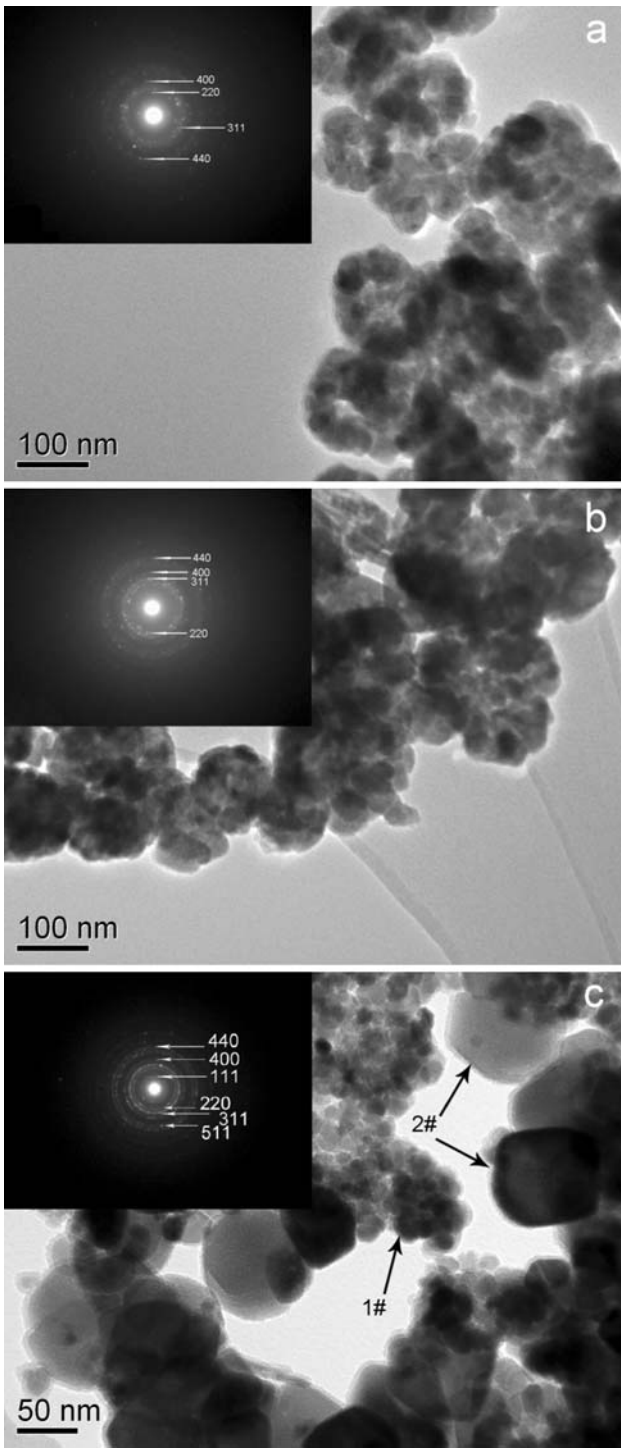

Fig. 3 TEM images of **a** S1, **b** S2 and **c** S3; the inset is the corresponding SAED pattern

the solution generates $Fe(OH)_2$ gels; subsequently upon addition of KNO_3 to this mixture, many of small magnetite nanoparticles (1# as shown in Fig. 3c) were formed through homogeneous nucleation. In contrast, if the Gla was not added, these small magnetite nanocages neither

demonstrate obvious growth nor do they aggregate due to the gel network structure in the gel solution, when several nucleation take place, the gels begin to flocculate during the aging period and form large Fe_3O_4 nanoparticles, the size range from 50 to 100 nm (2# as shown in Fig. 3c) [19]. Further detailed studies on the formation mechanism of the nanocages are currently under investigation.

Information on high-resolution morphologies and structures of the iron oxide nanocages can be gleaned from Fig. 4, and the HRTEM images obtained near the center region of hollow nanocages. Figure 4a shows that the Fe_3O_4 nanocages include three single crystalline … with an

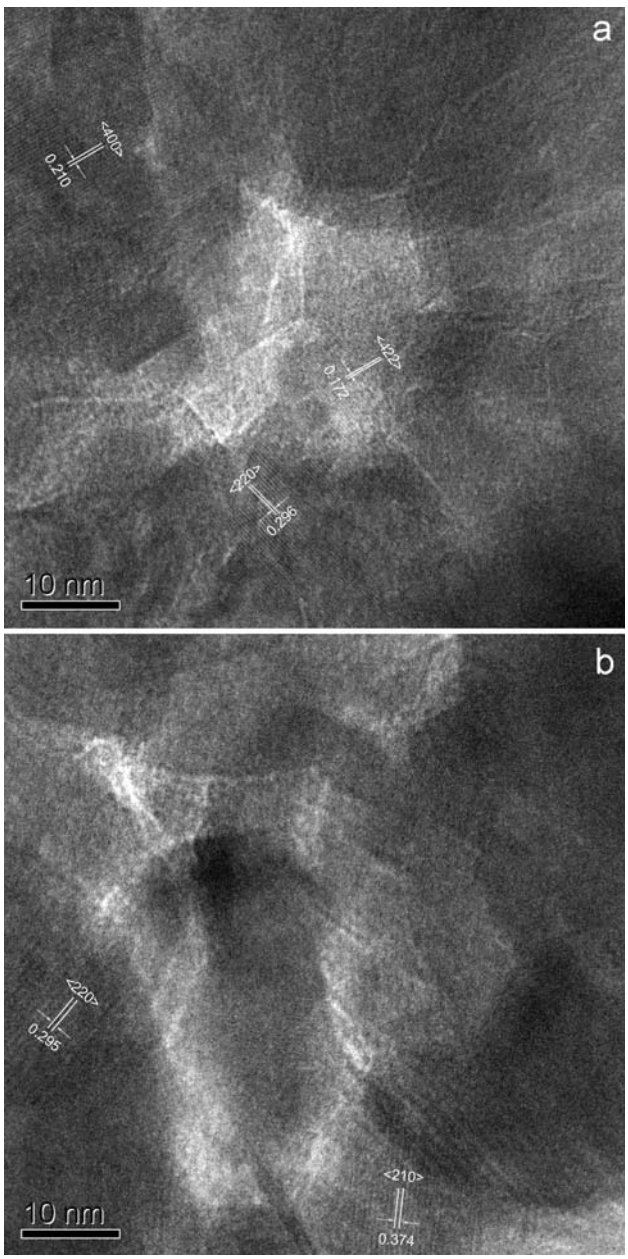

Fig. 4 HRTEM images of the center region of hollow Fe_3O_4 nanocages (**a**) and γ-Fe_2O_3 nanocages (**b**)

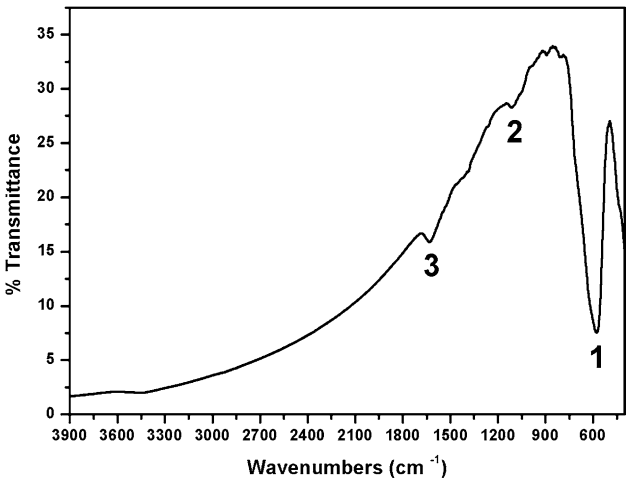

Fig. 5 FT-IR spectra of S1 (significant IR bands (1) 577.2 cm^{-1}; (2) 1,147.4 cm^{-1} (3) 1,633.0 cm^{-1})

interplanar spacing of 0.296 nm for the {220} plane, 0.210 nm for the {400} plane, and 0.172 nm for the {422} plane, respectively. Figure 4b shows that the γ-Fe_2O_3 nanocages include two single crystalline obviously with an interplanar spacing of 0.374 nm for the {210} plane and 0.295 nm for the {220} plane, respectively. The results further confirmed that the nanocages consist of randomly small iron oxide nanocrystals, and the nanocages present polycrystalline feature on the whole.

The attachment of Gla on the nanocage surface was confirmed by FT-IR spectroscopy (Fig. 5). The Fe–O stretching vibration is observed at 577.2 cm^{-1}, and C–O stretching vibration at 1,100–1,200 cm^{-1}; the bands that can be assigned to vibration of C–O are observed at 1,147.4 cm^{-1}, and the bands that can be assigned to vibration of COO^- group are observed at 1,633.0 cm^{-1} [20–22].

The magnetic properties of iron oxide nanocages were also investigated by SQUID. Hysteresis loop (Fig. 6A) measurements demonstrate that both samples exhibiting magnetization curves for the magnetic nanocages show no hysteresis; the forward and backward magnetization curves overlap completely and are almost negligible. Moreover, the magnetic nanocages have zero magnetization at zero applied field, indicating that they are superparamagnetic at room temperature. No remnant magnetism was observed when the magnetic field was removed [23]. This magnetic hysteresis phenomenon is also in agreement with previous reports by other groups [24–26]. The result reveals that these large nanocages are superparamagnetic is owing to the fact that they are composed of many small nanoparticles that show oriented aggregation into a hollow structure [27]. The saturation magnetization (M_S) of Fe_3O_4 nanocages was found to be 87 emu g^{-1} at 300 K and the M_S of γ-Fe_2O_3 nanocages was found to be 27 emu g^{-1} at 300 K.

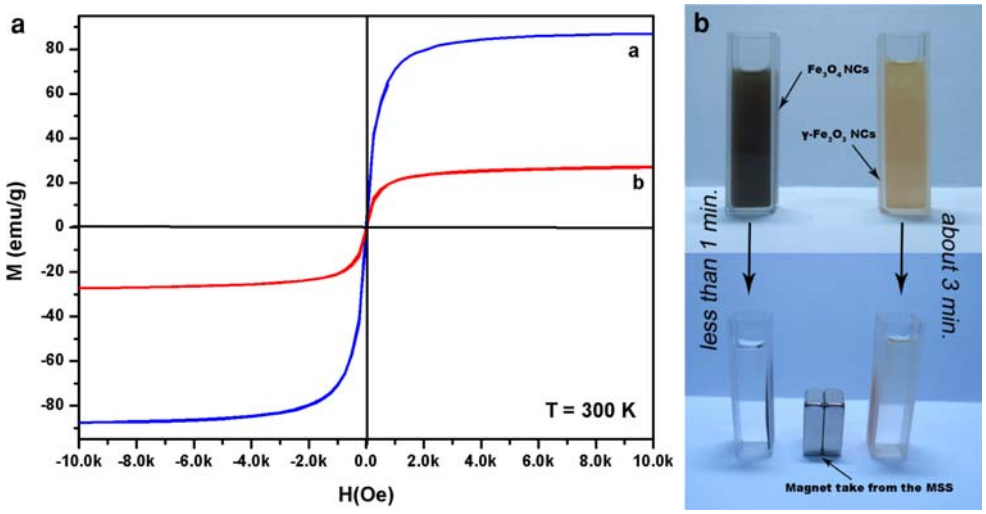

Fig. 6 Hysteresis loops (A) of Fe_3O_4 nanocages (*a*) and γ-Fe_2O_3 Nanocages (*b*); Photographs (B) of the Fe_3O_4 nanocages and γ-Fe_2O_3 nanocages (dispersed in ethanol solution) before and after magnetic separation by an external magnetic field (this magnet takes from the MSS)

It is noteworthy that the M_S of Fe_3O_4 nanocages is close to that of bulk magnetite (92 emu g^{-1}) [28]. Moreover, in the case of no hysteresis, the average size of the magnetic particle can be estimated from the initial susceptibility (χ_i), $\chi_i = (dM/dH)_{H\to 0}$ coming mainly from the largest particles. An upper limit for the magnetic size, D_m, may be estimated using the following formula [29]:

$$D_m = \frac{18k_BT}{\pi} \frac{\chi_i}{\rho M_s^2}$$

where ρ is the density of iron oxide nanoparticles, and Fe_3O_4 is 5.18 g/cm^3, and γ-Fe_2O_3 is 5.24 g/cm^3 and k_B is the Boltzmann constant. Thus the value of χ_i can be determined approximately. Using the values of saturation magnetization, M_S, obtained from the magnetization curve, the values of D_m were estimated: namely, the diameter of Fe_3O_4 nanocages was about 28 nm, and that of γ-Fe_2O_3 nanocages was about 42 nm, the result reveals that the iron oxide nanocages are composed … of small nanoparticles and the particle size as estimated by magnetization in agreement with the TEM images (Fig. 3) and HRTEM results (Fig. 4).

Furthermore, such excellent magnetic properties indicate that as-prepared nanocages have strong responsivity and can be separated easily from the solution with the help of an external magnetic force. Figure 6B shows photographs of the Fe_3O_4 nanocages and γ-Fe_2O_3 nanocages before and after magnetic separation by an external magnetic field. This figure also illustrates the facile, fast separation process of the nanocages during the experiments.

Conclusions

In summary, we have demonstrated a facile one-pot reaction approach in generating hollow iron oxide nanocages. In this method, Gla plays an important role in the formation of magnetite nanocages with hollow structure. The subsequent annealing will decrease the size of the central hole of hollow nanocages. The iron oxide nanocages prepared can be well dispersed in aqueous solution and show good stability. The magnetic property measurements of Fe_3O_4 nanocages show superparamagnetism with very high saturation magnetization close to the value of bulk Fe_3O_4 (92 emu g^{-1}). The synthetic strategy developed in this study may also be extended to the preparation of other magnetic nanoparticles, which also opens up new potential avenues for the nanostructural controlling and promising applications in various fields of nanotechnology.

Acknowledgments The author thanks the National Nature Science Foundation of China (No. 10775109), the Specialized Research Fund for the Doctoral Program of Higher Education (No. 20070486069), and the Young Chenguang Project of Wuhan City (No. 200850 731371) for financial support. The author thanks Associate Prof. H. -Y. Zhang of Tsinghua University for assistance with the SQUID measurements.

References

1. W. Wu, Q.G. He, C.Z. Jiang, Nanoscale Res. Lett. **3**, 397 (2008). doi:10.1007/s11671-008-9174-9
2. S.A. Corr, Y.P. Rakovich, Y.K. Gun'ko, Nanoscale Res. Lett. **3**, 87 (2008). doi:10.1007/s11671-008-9122-8
3. C.J. Tan, M.G. Chua, K.H. Ker, Y.W. Tong, Anal. Chem. **80**, 683 (2008). doi:10.1021/ac701824u
4. N. Kohler, C. Sun, J. Wang, M.Q. Zhang, Langmuir **21**, 8858 (2005). doi:10.1021/la0503451
5. B. Chertok, B.A. Moffat, A.E. David, F.Q. Yu, C. Bergemann, B.D. Ross, V.C. Yang, Biomater **29**, 487 (2008). doi:10.1016/j.biomaterials.2007.08.050
6. S.C. McBain, H.H.P. Yiu, A. El Haj, J. Dobson, J. Mater. Chem. **17**, 2561 (2007). doi:10.1039/b617402g
7. B. Steitz, H. Hofmann, S.W. Kamau, P.O. Hassa, M.O. Hottiger, B. von Rechenberg, M. Hofmann-Amtenbrink, A. Petri-Fink, J.

Magn. Magn. Mater. **311**, 300 (2007). doi:10.1016/j.jmmm.2006.10.1194
8. M. Tominaga, L. Han, L.Y. Wang, M.M. Maye, J. Luo, N. Kariuki, C.J. Zhong, J. Nanosci, Nanotechnology **4**, 708 (2004)
9. H.Y. Li, M.T. Klem, K.B. Sebby, D.J. Singel, M. Young, T. Douglas, Y.U. Idzerda, J. Magn. Magn. Mater. **321**, 175 (2009). doi:10.1016/j.jmmm.2008.08.082
10. D. Xi, X.P. Luo, Q.H. Lu, K.L. Yao, Z.L. Liu, Q. Ning, J. Nanopart. Res. **10**, 393 (2008). doi:10.1007/s11051-007-9263-1
11. A.K. Gupta, M. Gupta, Biomater **26**, 3995 (2005). doi:10.1016/j.biomaterials.2004.10.012
12. W. Wu, Q. He, H. Chen, J. Tang, L. Nie, Nanotechnology **18**, 145609 (2007). doi:10.1088/0957-4484/18/14/145609
13. A.-H. Lu, E.L. Salabas, F. Schüth, Angew. Chem. Int. Ed. **46**, 1222 (2007). doi:10.1002/anie.200602866
14. S. Laurent, D. Forge, M. Port, A. Roch, C. Robic, L.V. Elst, R.N. Muller, Chem. Rev. **108**, 2064 (2008). doi:10.1021/cr068445e
15. M.M. Titirici, M. Antonietti, A. Thomas, Chem. Mater. **18**, 3808 (2006). doi:10.1021/cm052768u
16. S. Peng, S. Sun, Angew. Chem. Int. Ed. **119**, 4233 (2007). doi:10.1002/ange.200700677
17. J. Yu, X. Yu, B. Huang, X. Zhang, Y. Dai, Cryst. Growth. Des. **9**, 1474 (2009). doi:10.1021/cg800941d
18. I. Mitov, Z. Cherkezova-Zheleva, V. Mitrov, Phys. Status Solidi. **161**, 475 (1997). doi:10.1002/1521-396X(199706)161:2<475::AID-PSSA475>3.0.CO;2-D
19. V.K. Lamer, R.H. Dinegar, J. Am. Chem. Soc. **72**, 4847 (1950). doi:10.1021/ja01167a001
20. M. Mikhaylova, D.K. Kim, C.C. Berry, A. Zagorodni, M. Toprak, A.S.G. Curtis, M. Muhammed, Chem. Mater. **16**, 2344 (2004). doi:10.1021/cm0348904
21. S. Si, A. Kotal, T.K. Mandal, S. Giri, H. Nakamura, T. Kohara, Chem. Mater. **16**, 3489 (2004). doi:10.1021/cm049205n
22. X.-C. Shen, X.-Z. Fang, Y.-H. Zhou, H. Liang, Chem. Lett. **33**, 1468 (2004). doi:10.1246/cl.2004.1468
23. H. Singh, P.E. Laibinis, T.A. Hatton, Langmuir **21**, 10500 (2005)
24. Y. Hou, S. Gao, T. Ohta, H. Kondoh, Eur. J. Inorg. Chem. 1169. (2004). doi:10.1002/ejic.200300779
25. Z. Li, Q. Sun, M. Gao, Angew. Chem. Int. Ed. **44**, 123 (2005). doi:10.1002/anie.200460715
26. K. Nakata, Y. Hu, O. Uzun, O. Bakr, F. Stellacci, Adv. Mater. **20**, 4294 (2008). doi:10.1002/adma.200800022
27. D. Nagao, M. Yokoyama, N. Yamauchi, H. Matsumoto, Y. Kobayashi, M. Konno, Langmuir **24**, 9804 (2008). doi:10.1021/la801364w
28. M. Yamaura, R.L. Camilo, L.C. Sampaio, M.A. Macêdo, M. Nakamura, H.E. Toma, J. Magn. Magn. Mater. **279**, 210 (2004). doi:10.1016/j.jmmm.2004.01.094
29. E.E. Carpenter, J. Magn. Magn. Mater. **225**, 17 (2001). doi:10.1016/S0304-8853(00)01222-1